

## RESEARCH ARTICLE

# A Marine Experiment Using Dielectric Elastomer Generators and Comparative Study with Actual Measured Values and Theoretical Values

Seiki Chiba<sup>1,\*</sup>  and Mikio Waki<sup>2</sup><sup>1</sup>Chiba Science Institute, Japan<sup>2</sup>Wits Inc., Japan

**Abstract:** Power generators using dielectric elastomer (DE) transducers are inexpensive, highly efficient, lightweight, stackable, and also easy to install. Therefore, it is considered optimal for an eco-energy society and is attracting attention as a renewable energy device. In particular, DE wave power generators are characterized by the fact that it is not limited by the direction and size of waves, which is a problem with existing wave power generation. This paper presents an accurate method for measuring the energy generated by a DE generator (DEG) and compares it with the theory value obtained by calculation. The electrode materials actually used in this study were a variety of carbon-based materials (including multi-wall carbon nanotube and single-wall carbon nanotubes), and the performance of DEs using these materials was compared. Furthermore, ocean experiments in actual sea areas using DEG were also conducted, and the energy conversion rate was calculated based on the electrical results.

**Keywords:** high-efficiency power generator, lightweight, large-deformation, flexible, SWCNT spray

## 1. Introduction

Electroactive polymer (EAP) artificial muscles are actuators that use electrical control to achieve movements that are similar to natural muscles. Those are often made of soft materials and are known as flexible actuators because of their soft movement. EAP artificial muscles can generally be classified into three categories: dry (electric field-responsive) types [1–3], wet (ionic) types [4–11], and other types [12–15]. In dry types, DEs attach electrodes to the upper and bottom of a polymer, and they are deformed using Coulomb force [1], and piezo polymers utilize piezoelectric phenomena [2, 3]. Wet types include those that use the movement of water molecules and ions within an elastomer [4, 8], those that combine an electrolyte membrane and thin metal electrodes [5–7], ionic polymer gels [9, 10], and carbon nanotubes [11]. Other types do not need electricity to deform, but they can use air, light, change in pH, heat, and magnetism to drive them like muscles [12–17]. For example, liquid crystals can be used to change the structure of polymers (using liquid crystals) [12]. These were classified as EAPs in this study.

The most promising of these is dielectric elastomer (DE), which is highly expected to be used as an actuator (DEA) [1, 18–22], sensor (DES) [1, 23–27], and generator (DEG) [1, 22, 28, 29]. Therefore, in recent years, many researchers have been conducting research and development on various fields including elastomer materials and their improvements for DEs [1, 22, 30–33], electrode materials [1, 22, 34, 35], high-voltage circuits, systems that combine them [1, 22, 28, 36–40], and their applications [1, 18, 22, 41–53].

\*Corresponding author: Seiki Chiba, Chiba Science Institute, Japan. Email: [chi.ba.jetpilot.seiki@gmail.com](mailto:chi.ba.jetpilot.seiki@gmail.com)

Incidentally, DE is a transducer technology invented in the late 1990s by Chiba et al. at Stanford Research Institute, USA (SRI) [54].

A DEG is different from typical electromagnetic induction power generation systems in that it uses electrostatic energy, which only functions as electrical energy only when a charge is flowing. To operate as a generator, electrostatic energy must be converted into electrical energy only when it is at its maximum. For example, static electricity energy is a high voltage, and the inability to accurately measure the voltage using ordinary measuring equipment is thought to be a major barrier. Thus, the impedance of the experimental setup and measurement systems is a key factor for accurately measuring the voltage and current.

In this study, the energy generation performance of four types of carbon-based electrode materials was compared, and an ocean power generation experiment was conducted using a buoy in an actual sea area using the electrode with the best performance. In addition, the energy generation value (J) theoretically calculated from the calculation formula was compared with the actual value measured using a system that could accurately measure the DEG output, and it was shown that the theoretical value could easily indicate the performance of the DEG.

## 2. Comparative Study of the Energy Measurement Value from the DEG and the Value from the Theoretical Formula

In this section, after the background of DE is briefly described, the DEG energy generation measurement method is considered, and the energy generation data obtained by driving the DEG are obtained. Subsequently, a theoretical calculation method for the amount of

energy generated was devised. The measured values were compared with the theoretical values.

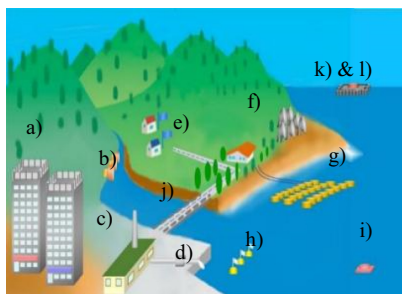
### 2.1. Background of DEs

As mentioned above, DE has a structure in which a thin polymer film is inserted between the expandable and contractible electrodes. When a potential difference is applied between the electrodes, static electricity causes the polymer film to shrink in the thickness direction and expand in the surface direction.

A significant feature of DE is that it can generate electricity by reversing the operating cycle of the DEA. That is, by distorting the elastomer, static electricity is generated and the elastomer itself becomes a capacitor. Microscopically, the elastic force of the elastomeric membrane pushes out the charge toward the electrodes (the membrane thickness increases in the contracted state), and the distance between each charge on the electrode decreases (the planar area of the electrode decreases in the contracted state). This change in charge increases the voltage difference, which results in increases in electrostatic energy.

Because this energy generation phenomenon does not depend on the speed of deformation of the DEA, DEG can easily utilize the vertical motion of waves, gentle flow of rivers, and vibrations generated by vehicles, buildings, etc., which have not been used much until now (see Figure 1) [22].

**Figure 1**  
Examples of locations where DE power plants could be constructed



- 1) DEG systems in which obtained electric power is consumed locally:
  - (a) Wind DEGs (including those installed on roofs of a building).
  - (b) Water mill DEGs.
  - (c) Waste energy DEGs.
  - (d) Drain generators.
  - (e) Wind DEGs for personal houses.
  - (f) Solar DEGs.
  - (g) Coastal type wave DEGs.
  - (h) Water flow DEGs.
  - (i) Ocean thermal energy conversion (OTEC) systems using DEGs.
  - (j) DEGs from vibrations (including power generation from vibrations caused by cars on roads and shaking of structures)
- 2) Huge DEG systems which are constructed on/in ocean.
  - (k) Wave DEGs on/in ocean.
  - (l) Hydrogen production site operated by the power of DEGs

### 2.2. Measurement of energy generated from DEG

As mentioned above, the DE generates electricity by moving in a direction opposite to the actuation in the generation. Charge appears on the elastomeric film when it was stretched (high capacitance). When

this film contracts (low capacitance), the elastic forces of the elastomer act against the electric field pressure, increasing electrical energy. This change in charge increases the voltage difference, which in turn increase the amount of electrostatic energy [1].

The capacitance  $C$  of the elastomer membrane can be written as follows.

$$C = \epsilon_0 \cdot \epsilon A/t = \epsilon_0 \cdot \epsilon \cdot b/t^2 \tag{1}$$

where  $\epsilon_0$  is the permittivity of free space,  $\epsilon_{is}$  is the dielectric constant of the elastomer membrane,  $A$  is the moving area of the elastomer membrane (i.e., the area of the variable capacitor),  $T$  is the thickness, and  $b$  is the volume of the membrane. In Equation (1), the volume of the elastomer is essentially unchanged, therefore  $At = b = const$ . The amount of electricity generated by a DE per cycle of expansion and contraction is related to the change in the capacitance of the DE and is expressed as follows.

$$\epsilon = 0.5C_1 V_b^2 \left( \frac{C_1}{C_2} - 1 \right) \tag{2}$$

where  $C_1$  and  $C_2$  are the capacitances of the DE in the stretched and contracted states, respectively, and  $V_b$  is the bias voltage.

Considering the change with respect to voltage, the charge  $Q$  in the DE can be considered constant in the basic circuit over a short period. Because  $V = Q/C$ , the contracted state voltage  $V_2$  can be written as follows when the stretched state voltage  $V_1$  is used.

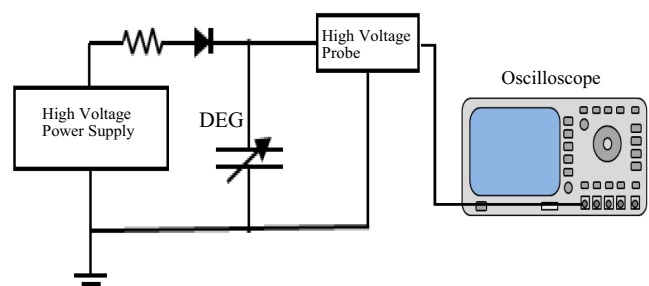
$$V_2 = \frac{Q}{C_2} = \left( \frac{C_1}{C_2} \right) \left( \frac{Q}{C_1} \right) = \left( \frac{C_1}{C_2} \right) \cdot V_1 \tag{3}$$

Because  $C_2 < C_1$ , according to the energy theory proposed by Chiba et al., the voltage in the contracted state is higher than that in the stretched state [22]. These results were confirmed experimentally. As described above, a DEG generates electricity by discharging electricity when it is pushed in and discharging it when it is released. According to Equation (2), the larger the difference between  $C_1$  and  $C_2$ , that is, the difference between the capacitance when stretched and the capacitance when contracted, the more power is generated; therefore, the smaller the thickness  $t$  of the elastomeric membrane, the large the capacitance. Thus, the larger the capacitance and the higher the rate of change during contraction, the greater is the amount of power generation.

The energy ( $\epsilon$ ) delivered by DEG can be calculated using the above formula by following steps [22].

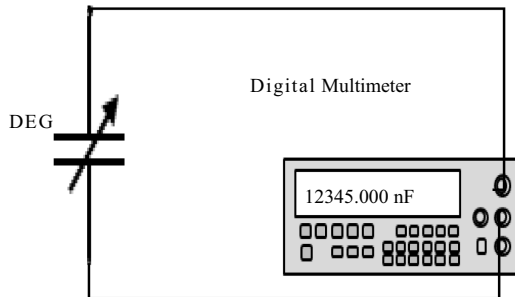
- 1) The voltage ( $V_2$ ) between the electrodes of the upper and lower sides of the DEG in the contracted state was measured for each wave frequency using an oscilloscope (see Figure 2).

**Figure 2**  
Circuit for measuring the DE voltage at a contracted state



- 2) The capacitance ( $C_2$ ) of the transducer in the contracted state is measured with a multimeter (see Figure 3).

**Figure 3**  
Circuit for measuring the capacitance of a DEG at a contracted state



- 3) Using the values of Equations (2) and (3), and  $C_2$  and  $V_2$ , the amount of energy generation is calculated as follows:

- a. The relationship  $C_1 = V_2 C_2 / V_1$  is obtained from Equation (2) (4)
- b. Subsequently by introducing  $C_1$  into Equation (3), the generated electric energy can be obtained:

$$\epsilon = 0.5 V_1 V_2 C_2 \left\{ \left( V_2 / V_1 \right) - 1 \right\} \quad (5)$$

- c. Using Equation (5) and the values of  $C_2$  and  $V_2$ , the energy generated at the frequency of each wave of the transducer can be calculated.

The structure of the diaphragm-type DEG used in the experiment to measure the amount of energy generated using the DEG and a discussion on the power generation are described below.

A diaphragm-type DEG has the shape shown in Figure 4(a) and is pushed by an external force (pushing by hand) to generate

electricity [22]. A photograph of this device and its cross-section are shown in Figure 4(b) and (c), respectively.

In this experiment, carbon black, MWCNTs (made in China), and SWCNTs (ZEONANO®-SG101) were used as electrodes. In addition, the above SWCNTs were separated using a swing rotor ultracentrifuge (S52ST, Hitachi Koki) to obtain “selected SWCNTs” [1]. The separation was performed at 52,000 rpm for 24 h. Thus, SWCNTs with small diameter were selected.

To facilitate electrode fabrication, a CNT solution for spraying was prepared by mixing dispersed CNTs with a binder. The CNT dispersion was prepared by first adding CNTs and a 2 wt% sodium cholate solution to a dispersion medium and then dispersing the CNTs using an ultrasonic homogenizer [27]. This solution was placed in a spray can and used as a spray. The carbon blacks were dissolved in MEK. These carbon-based materials were sprayed to create electrodes with a thickness of 50  $\mu\text{m}$ . The diameter of these DEGs was 8 cm (see Figure 4(a) & (b)), and the elastomer used was acrylic (3MVBH4910). The weight of the acrylic membrane was 2.8 g.

The usage of electrodes with good conductivity drastically improved the energy generation performance of DEs, as shown in Table 1.

### 2.3. Energy values from theoretical formula

First, the parameters required to calculate the amount of energy generation are the surface areas  $A$  and the membrane thickness  $t$  according to Equation (2). As shown in Figure 4(c), the inside of the diaphragm DEG has a push part and an elastomer membrane part, and the elastomer membrane is in the shape of a disk with a hole in the center (see Figure 3). First, the size of the elastomer (see Figure 5) and the surface area  $A_0$  of the elastomer membrane inside the diaphragm generator are determined. The formula for calculating  $A_0$  can be expressed as follows.

$$A_0 = \pi(R^2 - r^2) \quad (6)$$

In addition, in the cross-section of the elastomer at the bottom of Figure 4, the surface area of the elastomer membrane when the generator switch is pushed in by  $d$  mm is expressed by Equation (7).

**Figure 4**

**Diaphragm-type DEG device. (a) A photograph of diaphragm-type DEG. (b) A photograph of this device. (c) Its cross-section**

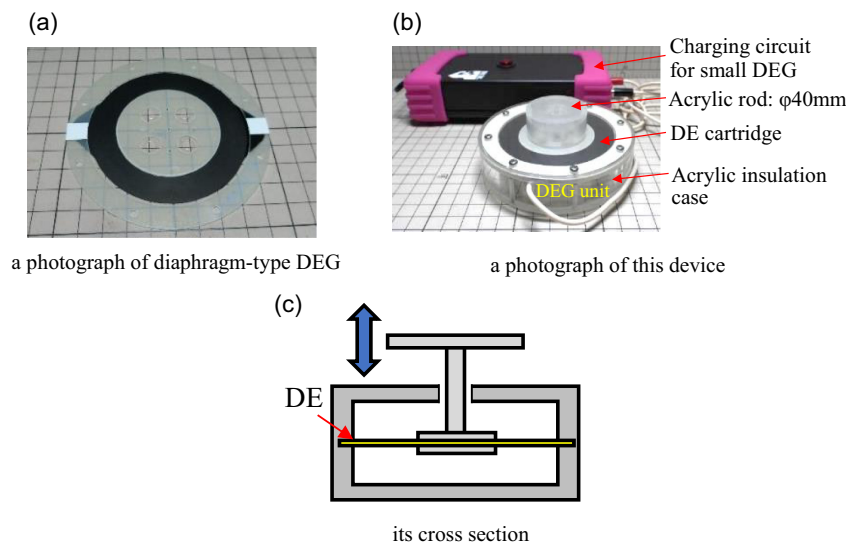
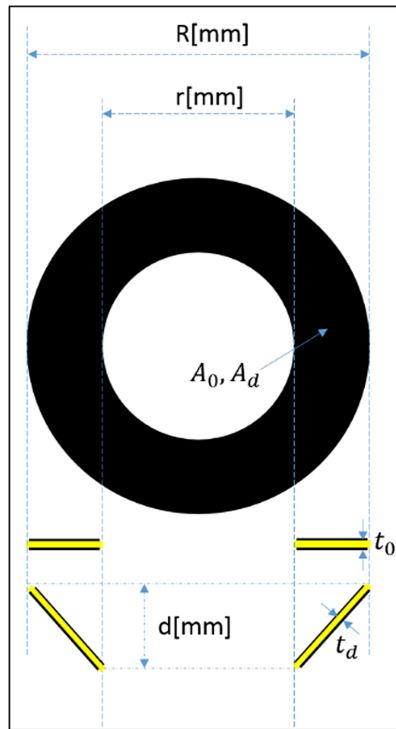


**Table 1**  
**Comparison of measured values and theoretical values**

Electrode type	Energy generated (mJ)	Theoretical value (mJ)
Carbon black	45.68	45.77
MWCNT	74.11	74.79
SWCNT	105.06	105.88
Selected SWCNT	136.58	137.65

Note: The above SWCNTs were furthermore separated using a swing rotor ultracentrifuge to obtain selected SWCNTs. The theoretical energy generation yields of MWCNTs, SWCNTs, and selected SWCNTs are explained in Section 2.4. Consideration regarding the structure of diaphragm-type DEG and its energy generation amount (actually measured values and theoretical values).

**Figure 5**  
**The cross-sectional view of the elastomer**



$$A_d = \pi(R+r)\sqrt{(R-r)^2 + d^2} \quad (7)$$

The stretching ratio  $\lambda_d$  is introduced here:

$$\lambda_d = \frac{A_d}{A_0} = \frac{\pi(R+r)\sqrt{(R-r)^2 + d^2}}{\pi(R^2 - r^2)} = \frac{\sqrt{(R-r)^2 + d^2}}{R-r} \quad (8)$$

When the stretching ratio  $\lambda_d$  is introduced, the volume  $b$  of the elastomer membrane is constant; thus,  $t_d$  becomes:

$$\begin{aligned} t_d &= \frac{b}{A_d} = \frac{b}{\pi(R+r)\sqrt{(R-r)^2 + d^2}} = b \times \frac{A_0}{A_0 \cdot A_d} = t_0 \times \frac{1}{\lambda} \\ &= \frac{R-r}{\sqrt{(R-r)^2 + d^2}} \cdot t_0 \end{aligned} \quad (9)$$

Substituting this result into Equation (1), the capacitance  $C_d$  is

$$C_d = \epsilon_0 \epsilon \cdot \frac{A_d}{t_d} = \epsilon_0 \epsilon \cdot \frac{A_0 \lambda^2}{t_0} = \epsilon_0 \epsilon \cdot \frac{A_0((R-r)^2 + d^2)}{t_0(R-r)^2} \quad (10)$$

This results in

$$\frac{C_d}{C_0} = \lambda_d^2 \quad (11)$$

and is found and substituted into Equation (2) along with the result of Equation (10), the equation for the generation amount becomes as follows.

$$\epsilon_d = 0.5 \times C_d V_b^2 (\lambda_d^2 - 1) \quad (12)$$

According to Equations (11, 12) becomes

$$\epsilon_d = 0.5 \times C_0 V_b^2 \lambda_d^2 (\lambda_d^2 - 1) \quad (13)$$

From the above, it can be seen that the power generation amount  $\epsilon_d$  is proportional to the  $\lambda_d$  to the fourth power. In addition, because  $\lambda_d^2$  is proportional to  $d^2$ , the energy generation  $\epsilon_d$  is proportional to  $d$  to the fourth power.

The data for the calculation are shown below.

$$\begin{aligned} \epsilon_0 &= 8.85 \times 10^{-12} \\ \epsilon &= 4.8 \\ t_0 &= 0.16 \text{ mm} \\ d &= 12 \text{ mm} \\ R &= 80 \text{ mm} \\ r &= 40 \text{ mm} \\ d_0 &= 12 \text{ mm} \\ V_b &= 3000 \text{ V} \end{aligned}$$

As a result of the calculation using the above values, the actual measured and theoretical values almost matched (see Table 1 and Figure 6).

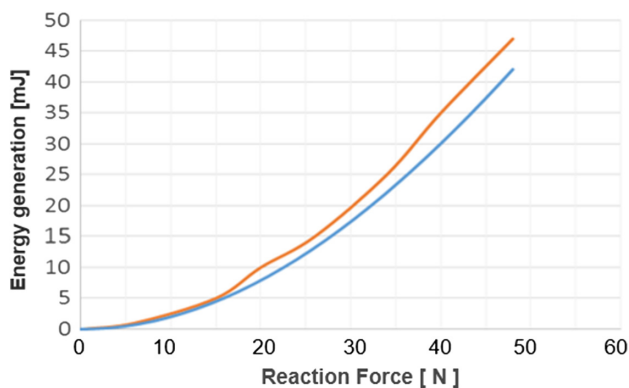
#### 2.4. Consideration regarding the structure of diaphragm-type DEG and its energy generation amount

The structure of the diaphragm-type DEG used in this research and experiment, as well as its measured electrical capacity and theoretical values, is discussed below.

As shown in Figure 6, if this method is used, it is possible to predict the amount of energy generation to some extent for small diaphragm types. When the load was small, it matched the measured value; however, as the external force (load) increased, there were some errors with the measured value. This is because the accuracy of the formula for calculating the thickness of the DE during deformation was low, which affected the stretching ratio. In addition, we did not take into account the differences in the electrode materials used in the experiment.

When a DEG generates electricity, it is important to know how much the membrane deforms in the vertical, horizontal, and torsional

**Figure 6**  
Comparison of measured DEG energy generation amount (red line) and theoretical value (blue line)



directions as well as how much the membrane thickness changes. Incidentally, the  $t_0$  of the drape DEG with a diameter of 260 mm and a height of 120 mm created four years ago by authors was 0.19 mm, while the  $t_0$  of the diaphragm DEG created this time was 0.16 mm [22]. That is, it is 1.19 times the  $t_0$  of the draped DEG. In the case of  $d$ , the draped DEG is 60 mm, while the  $d$  of the diaphragm DEG is 12 mm, so the  $d$  of the draped DEG is 5 times larger. In other words, the drape is 5.95 times larger than the diaphragm in total. For comparison with the diaphragm DEG, the energy data of a draped DEG with a diameter of 260 mm and a height of 120 mm are shown in Table 2 [22].

**Table 2**  
Difference in energy obtained when changing the electrode material

Type of electrode	Energy obtained [mJ]
Carbon black <sup>1</sup>	274
Multi-walled carbon nanotube	445
Single-walled carbon nanotube	630
Selected SWCNT <sup>1</sup>	819

<sup>1</sup> Carbon blacks and MWCNTs are manufactured in companies in the United States. SWCNTs used were ZEONANO®-SG101, and Selected SWCNTs were created based on the SWCNTs.

Compared with the diaphragm-type data in Table 1, the values of carbon black, MWCNT, SWCNT, and selected SWCNT are about 6 times higher, which is almost the same as the values above. Because there is still little comparative data, it is difficult to draw a clear conclusion, but the values of  $t_0$  and  $d$  are considered to be promising factors for estimating the theoretical amount of energy generated. Based on these results, the theoretical amount of energy generated by the diaphragm DEG with a CNT electrode is shown in Table 1. The results were almost the same as the actual measured values.

Furthermore, as the DEG size increases, the film may not return uniformly during the process of returning to its original length/shape. In the future, it will be necessary to verify the size of the DEG membrane and its energy generation performance. In addition, DEGs have various shapes, such as diaphragm, drape, sheet, folding, and roll shapes; therefore, developing calculation methods

tailored to these shapes will be extremely useful in the future development of business devices using DEGs.

As mentioned above, one way to increase the energy production of a DEG is to choose a material with higher conductivity of the electrodes. A comparative experiment was conducted using carbon black, MWCNT, SWCNT, and selected SWCNT, and it was clear that the amount of energy generated increased in the order of higher conductivity (see Table 1). Carbon grease has been used as an electrode, but it is not very impressive. However, during experiments, grease sometimes leaks, which poses a major durability problem [27]. In addition, its conductivity was much lower than that of carbon black. In this experiment, we successfully sprayed various carbon materials using optimal dispersion solvents. Using this spray, electrodes of any shape can be fabricated. Furthermore, the electrode can be applied to a considerably thinner thickness. In this experiment, it was set as 50  $\mu\text{m}$ . The thinner electrodes deform with less external force, which increases the amount of power generated. Recently, research has been conducted using liquid metal for DE electrodes; however, in this case, as with grease, there are concerns that if the experiment is repeated several times, there will be leakage or damage to the electrodes owing to high voltage.

In this experiment, a swing rotor ultracentrifuge to further separate the SWCNTs was used and obtain “selected SWCNTs” with even more conductivity. This was performed to obtain smaller diameter CNTs, and the resulting SWCNTs were 1–2 nm. When thinner diameters of CNTs are applied, the dispersibility of CNTs as electrodes increases, and it seems that they can function satisfactorily as electrodes even if they are significantly deformed. Cylindrical materials such as CNTs can produce larger changes because they are more likely to be in contact with the materials even when stretched. The selected SWCNTs are CNTs with a thinner diameter, and the SWCNT density in the electrode is thought to be higher than the SWCNTs mentioned above. Thus, there is a high possibility that they will be in contact somewhere, even if they are stretched significantly. The above mechanism can be explained as follows using a carbon black electrode as the example [1]. Figure 7 shows the photograph of a DEA using the carbon black as an electrode, with (a) the power OFF and (b) ON. As shown in the schematic diagram of Figure 8, the power is off, so the electrode is not pulled. Therefore, light does not pass through. In the operating state, the electrode is pulled, and a certain amount of carbon black particles are pulled away, so the light passes through those parts. However, not all the particles are separated, so it functions as a DEA. 3M/4905 is used in this DEA, and the thickness of the electrode is very thin at 40  $\mu\text{m}$ .

However, the DEG film is already very thin, and there is currently a limit to the amount of change in  $t$  due to external force; therefore, a smart way to ensure power generation is to incorporate multiple elastomer membranes in inside the DEG. The four DEGs were grouped together in one layer in this experiment. This method is convenient, but if too many devices are stacked, the force driving the DEG will increase considerably. Therefore, in case where the external force is not very large, it is better to distribute devices with a reduced number of stacked layers.

In this experiment, only 3M acrylic was used as the elastomer. This acrylic material is softer than other commercially available elastomers and can generate large deformations (power generation) even with small external forces [27]. Currently, various elastomers are being synthesized; however, 3M's elastomer appears to show the best results to date. Hydrogen nitrile rubber (HNBR) is also an interesting material, but its elongation should be slightly improved while maintaining its strength [1].

**Figure 7**  
Light transmittance change of a DEA using carbon black. (a) Power off. (b) Power on

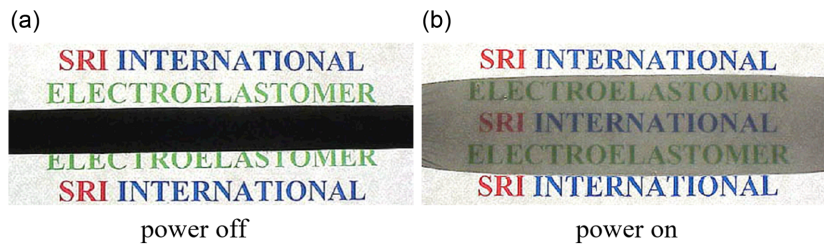
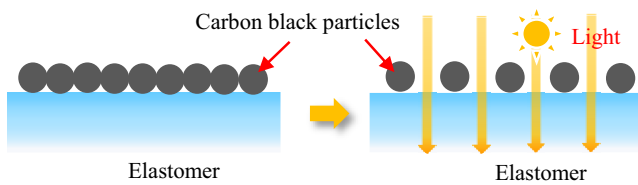


**Figure 8**  
A state in which carbon black particles are lined up as an electrode on the elastomer and the state in which the elastomer is being elongated



In addition, there is still much to be investigated, such as the optimal voltage and pre-stretch for each material, and future research and development will be expected.

### 3. Applying DEG to Marine Experiments in Actual Sea Areas

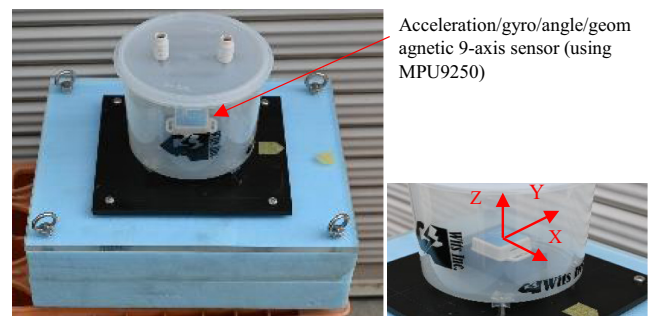
Using the DEG used in the above experiment, we conducted a power generation experiment in an actual sea near an aquaculture raft on the coast of Sakaide City, Kagawa Prefecture in Japan (Figure 9). Sakaide is located at these coordinates: (34°22'49.1"N 133°55'18.3"E).

**Figure 9**  
Photo of aquaculture raft



Figure 10 shows the handmade buoy used in the experiment. The float used in the experiment was made of urethane foam and measured 320 mm × 270 mm × 100 mm. A power generation unit consisting of a diaphragm DEG incorporating 1.4 g of acrylic (3M VHB4910) DEG moving vertically in response to waves

**Figure 10**  
The handmade buoy used in the experiment. Having the size of 320 mm × 270 mm × 100 mm



was positioned in the center of the buoy on the water surface (see Figure 10). An acceleration, gyro, angle, and geomagnetic 9-axis sensor (using MPU9250) was incorporated into the buoy, and a simple displacement amount was determined from the acceleration. This displacement amount was calculated by double integrating the measured acceleration. The standard gravitational acceleration was taken as 9.8 m/s<sup>2</sup>. The frequency was also determined by Fourier analysis. However, in this experiment, the buoyancy of the floating body was insufficient; therefore, it was not possible to use the above system with four DEGs. Increasing the number of DEGs requires an increase in the capacitor size of the measurement electrical circuit. In addition, because four cases are required to store the DEG, the only option is to reduce the weight. Therefore, we decided to use only two DEGs. The electrodes of this DEG were fabricated using the selected SWCNTs. The DEG has a maximum energy production capacity of approximately 68.29 mJ per stroke. This is because the weight of the DEG used here was 1.4 g, which is half the weight of the DEG shown in Table 1. Incidentally, the external force required for maximum energy generation output was 22.54 N. A buoy was moored from a boat anchored near the raft (Figure 11).

In addition to the DEG, this buoy was equipped with acceleration, gyro, angle, and geomagnetic 9-axis sensors. The wave observation results (displacement and frequency obtained by 3-axis synthesis) are shown in Figures 12(a) and (b). The Fourier analysis conditions were the number of data( $n$ ) = 256 and time step( $d_t$ ) = 0.1 s. Furthermore, the maximum frequency of the synthesized displacement amount was 0.98 Hz. The maximum energy generation amount was 39.767 mJ when the wave height was 3 cm and the wave period was 0.98.

**Figure 11**  
The buoy moored to a small boat floating next to the raft



**3.1. Consideration of data obtained from buoy power generation in the ocean**

The maximum energy generation obtained in this experiment was 39.767 mJ using two DEGs, when the wave height was 3 cm. This was because the four DEG devices used in the above experiment could not be used because of the buoyancy of the floating body used in this study. First, to increase the amount of energy generated by this system, it is necessary to provide sufficient buoyancy relative to the weight of the

DEG system. In addition, in this experiment, a 20 kg weight was simply sunk to the seabed and the weight was linked to the DEG inside the buoy; however, in order to reliably obtain electricity from the power of the waves, it is necessary to properly anchor it to the seabed using a mooring wire. Alternatively, the amount of energy generation can be increased by installing a sufficiently large plate under the buoy and connecting the plate and DEG with a mooring wire (see Figure 13) [22].

As Miyazaki et al. pointed out, existing wave power generation systems are limited by the direction and size of waves [55], but DEG buoy power generation can generate electricity with waves as small as 3 cm. Because of its shape, it can handle waves in all directions. One point is that in the case of buoy power generation, it is necessary to consider the arrangement of buoys. This is because waves can cause interference between buoys, thereby reducing the power generation capacity. To avoid this, it would be better to use an oscillating water column (OWC) that incorporates a DEG instead of a buoy (Figure 14) [1, 22, 53]. In this ocean experiment, a weight of 20 kg was attached to the buoy and sunk to the seabed. Thus, it is believed that the shape of the seabed affects the power generation performance of the buoy (including the case of attached plates shown in Figure 13) or the OWC. Srinu et al. evaluated the effect of seabed undulations on the efficiency of an OWC device [56]. Mohapatra also investigated the hydrodynamic performance of a shore-fixed OWC device in the presence of convex, concave, and sloped step-type bottom profiles is investigated [57].

Even if a large number of OWCs are placed in the front, back, left, and right, there is a collector; therefore, the DEG can generate

**Figure 12**  
Wave observation results. (a) Displacement amount. (b) Frequency obtained by 3-axis synthesis

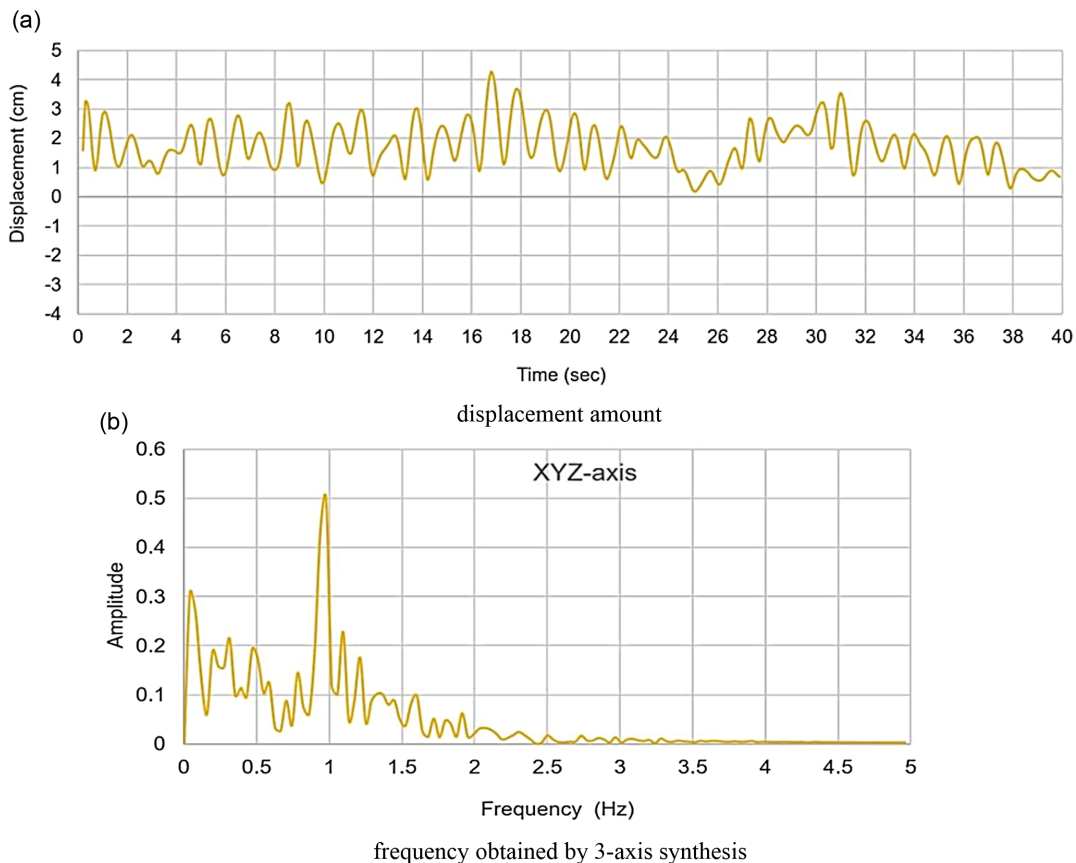


**Figure 13**  
A buoy with plate installed

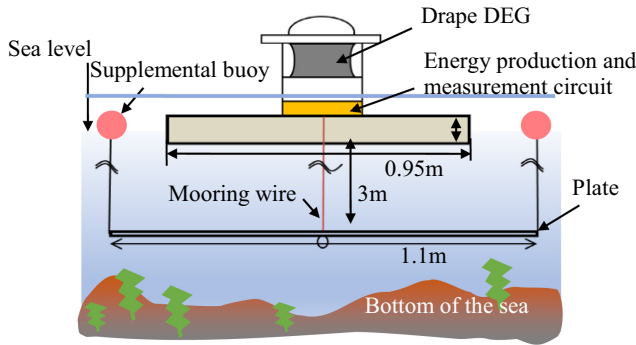
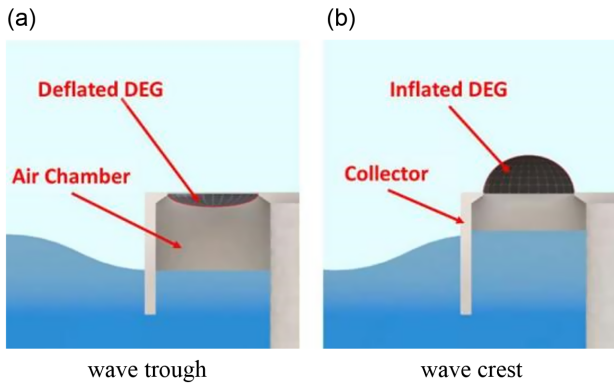


**Figure 14**  
OWC wave DEG. (a) Wave trough. (b) Wave crest



electricity without being affected by the surrounding environment (see Figure 14(b)).

Based on the above experimental results, the energy conversion rate was calculated as follows. The average wave energy per unit width ( $\epsilon$ ) was obtained by adding the potential energy ( $\epsilon_p$ ) to the kinetic energy ( $\epsilon_k$ ):

$$\epsilon = \epsilon_p + \epsilon_k = \frac{1}{8} \rho g H^2 \quad (14)$$

where  $\rho$  is the density of water (999.97 kg/m<sup>3</sup>),  $g$  is the gravitational acceleration (9.8 m/s<sup>2</sup>) and  $H$  is the wave height (m). Because the average wave energy in a wave period ( $\mathcal{W}$ ) corresponds to the wave power, it can be expressed by Equation (15) by multiplying the group velocity of wave ( $C_g$ ) and wave energy ( $\epsilon$ ):

$$\mathcal{W} = \frac{\rho g H^2}{8} \cdot \frac{\sigma}{k} \cdot \frac{1}{2} \left\{ 1 + \frac{2kh}{\sinh 2kh} \right\} = \epsilon C_g = \epsilon C \quad (15)$$

where  $n$  is the fraction of the group velocity of the wave ( $C_g$ ) against the phase velocity of the wave ( $C$ ), which is expressed by Equation (16):

$$n = \frac{C_g}{C} = \frac{1}{2} \left\{ 1 + \frac{2kh}{\sinh(2kh)} \right\} \quad (16)$$

where  $h$  is the water depth (m) and  $k$  is the wave number (m<sup>-1</sup>).  $k$  is expressed by the following equation:

$$k = \frac{2\pi}{L} \quad (17)$$

where the wavelength ( $L$ ) is expressed by Equation (18):

$$L = \frac{gT^2}{2\pi} \tanh \left( 2\pi \frac{h}{L} \right) \quad (18)$$

where  $T$  is the wave period (s).

The wavelength ( $L$ ) can be approximately expressed by Equation (19):

$$L \approx \frac{gT^2}{2\pi} \tanh \left\{ 2\pi \sqrt{\frac{h}{gT^2}} \left( 1 + \sqrt{\frac{h}{gT^2}} \right) \right\} \quad (19)$$

The phase velocity of the wave ((m/s)) is expressed by Equation (20):

$$C = \sqrt{\frac{g}{k} \tanh kh} \quad (20)$$

The group velocity of wave ( $C_g$  (m/s)) can be expressed by the following Equation (21) by using Equations (16 and 19):

$$C_g = C \cdot \frac{1}{2} \left\{ 1 + \frac{2kh}{\sinh 2kh} \right\} \quad (21)$$

The water depth ( $h$ ) of the experimental sea area was 3 m. The wave height and period are 0.03 m and 0.98 s, respectively. The energy of the wave per unit width ( $\mathcal{W}$ ) was based on the above experimental results, the energy conversion rate was calculated as wave energy for the floating body width is 5.72 W/m  $\times$  0.32 m = 1.83 W.

For the experimental condition of the wave height is 0.03 m and the wave period is 0.98 s, the electric energy generation ( $\epsilon_g$ ) is 39.767 mJ. As a result, the electric energy ( $\mathcal{W}_g$ ) was  $\mathcal{W}_g = 39.767$  mJ/0.98 s = 40.579 mW. Thus, the energy conversion efficiency ( $\eta$ ) is  $\eta = 40.579$  mW/1.83 W = 0.02217 (2.217%). It is concluded that 2.217% of wave energy is converted to electric energy in the experiment for the wave height of 0.03 m and the wave period is 0.98 s. This means that, theoretically, placing 45 more DEGs per meter could absorb 100% of this wave energy and convert it into electrodes. The size of this DEG is small enough, so a large number of DEGs can be installed, and it can generate electricity 24 h a day, 365 days a year; if it is stored in a secondary battery, a considerable amount of electricity can be used.

As mentioned above, the energy conversion efficiency of the DEG is relatively small compared to the wave energy. However, the maximum energy generation capacity of the DEG was 68.29 mJ and 39.767 mJ at a wave height of 3 cm. Therefore, the energy generation efficiency of the DEG is 58.2%. In another experiment conducted by the authors using a wave tank 30 m long, 0.6 m wide, and 1.5 m deep, 90.6% was recorded at a wave height of 6 cm [54]. By the way, the champion data for LNG-fired power generation were 63.6% achieved by Tohoku Electric Power in 2023 [58]. However, existing wave power generation systems are limited by the direction and size of the waves, and the systems are complex, making construction costs very high. As Adderlini et al. pointed out, the levelized energy cost of the existing system has not yet reached a level that can compete with fossil fuel power plants [59]. In other words, the power generation efficiency is still low. Recently, the Hiratsuka Wave Power Plant in Japan claimed to have achieved 50% efficiency when waves were 150 cm high [60].



However, this can only be achieved if the waves are set to strike the reflector perpendicularly. The system uses a wave reflector that rocks back and forth with the energy of the incoming waves, driving a hydraulic cylinder that drives a permanent magnet generator, which converts the energy into electrical energy.

#### 4. Conclusion

In this study, a comparison was made between the energy generation value theoretically calculated from the calculation formula and the actual value measured using a system that can accurately measure the DEG output. It was found that the theoretical value can also almost indicate the performance of the DEG. In addition, the energy generation performance using four types of carbon-based electrode materials (carbon black, MWCNT, SWCNT, and selected SWCNT) was compared and the electrode with the best performance was used on a buoy in the actual sea. As a result, an offshore power generation experiment was conducted, and its usefulness was demonstrated.

#### Funding Support

We would like to thank M. Uejima and H. Uchida of the ZEON Corporation for providing SWCNTs (ZEONANO®-SG101) free of charge for carrying out our experiments.

#### Ethical Statement

This study does not contain any studies with human or animal subjects performed by any of the authors.

#### Conflicts of Interest

The authors declare that they have no conflicts of interest to this work.

#### Data Availability Statement

Data available on request from the corresponding author upon reasonable request.

#### Author Contribution Statement

**Seiki Chiba:** Conceptualization, Methodology, Software, Validation, Formal analysis, Investigation, Resources, Data curation, Writing – original draft, Writing – review & editing, Visualization, Supervision, Project administration, Funding acquisition. **Mikio Waki:** Methodology, Software, Validation, Formal analysis, Investigation, Resources, Data curation, Writing – original draft, Writing – review & editing, Visualization.

#### References

- [1] Chiba, S., Waki, M., Takeshita, M., & Ohya, K. (2024). Examination of factors to improve the performance of dielectric elastomer transducers and their applications. *Smart Materials and Structures*, 33(6). <https://doi.org/10.1088/1361-665X/ad4759>
- [2] Kurita, Y., Sugihara, F., Ueda, J., & Ogasawara, T. (2010). MRI compatible robot gripper large-strain piezoelectric actuator. *The Japan Society of Mechanical Engineers*, 76(761), 132–141. <https://doi.org/10.1299/kikaic.76.132>
- [3] Gross, B. (1944). Experiments on electrets. *Physical Review Journals Archive*, 66, 26. <https://doi.org/10.1103/PhysRev.66.26>
- [4] Takagi, K. (2019). Polymer actuators and science for soft robotics. *The Robotics Society of Japan*, 37(1), 38–41. <https://doi.org/10.7210/jrsj.37.38>
- [5] Boldini, A., Bardella, L., & Porfiri, M. (2020). On structural models for ionic polymer metal composites. In *Proceedings of the SPIE 11375, Electroactive Polymer Actuators and Devices (EAPAD) XXII, 113751B*. <https://doi.org/10.1117/12.2558302>
- [6] Suzumori, K., Nabae, H., Asaka, K., & Horiuchi, T. (2020). Applying IPMC to soft robots. In *Proceedings of the SPIE 11375, Electroactive Polymer Actuators and Devices (EAPAD) XXII, 113750A*. <https://doi.org/10.1117/12.2557021>
- [7] Oguro, K., Fujiwara, N., Asaka, A., Onishi, K., & Sewa, S. (1999). Polymer electrolyte actuator with gold electrodes. In *Proceedings of the SPIE; Electroactive Polymer Actuators and Devices*, 3669, 64–71. <https://doi.org/10.1117/12.349698>
- [8] Otero, F., & Sansiñena, J. (1998). Soft and wet conducting polymers for artificial muscles. *Advanced Materials*, 10(6), 491–494. [https://doi.org/10.1002/\(SICI\)1521-4095\(199804\)10:6<491::AID-ADMA491>3.0.CO;2-Q](https://doi.org/10.1002/(SICI)1521-4095(199804)10:6<491::AID-ADMA491>3.0.CO;2-Q)
- [9] Osada, Y., Okuzaki, H., & Hori, H. (1992). A polymer gel with electrically driven motility. *Nature*, 355, 242–244.
- [10] Katchalsky, A. (1949). Rapid swelling and deswelling of reversible gels of polymeric acid by ionization. *Experimentia*, 5, 19–32.
- [11] Baughman, R., Cui, C., Zakhidov, A., Iqbal, Z., Barisci, J., Sprinks, G., . . . , & Kertesz, M. (1990). Carbon nanotube actuators. *Science*, 284, 1340–1344. <https://doi.org/10.1126/science.284.5418.1340>
- [12] Ratna, B., Ratha, D., Laurence, T., & Keller, P. (2001). Liquid crystalline elastomers as artificial muscles: Role of side chain-backbone coupling. In *Proceedings of the SPIE 4329; Smart Structures and Materials 2001: Electroactive Polymer Actuators and Devices*, 4329, 432651. <https://doi.org/10.1117/12.432651>
- [13] Chou, P., & Hannaford, B. (1994). Static and dynamic characteristics of McKibben pneumatic artificial muscles. In *Proceedings of the IEEE International Conference on Robotics and Automation*, 281–286. <https://doi.org/10.1109/ROBOT.1994.350977>
- [14] Smots, G. (1995). New developments in photochromic polymers. *Journal of Polymers Science: Polymers Chemistry Edition*, 13, 2223–2231. <https://doi.org/10.1002/pol.1975.170131005>
- [15] Tobushi, H., Hayashi, S., & Kojima, S. (1992). Mechanical properties of shape memory polymer of polyurethane series: Basic characteristics of stress-strain-temperature relationship. *JSME International Journal, Series I, Solid Mechanics, Strength of Materials*, 35(3), 296–302. [https://doi.org/10.1299/jsmea1988.35.3\\_296](https://doi.org/10.1299/jsmea1988.35.3_296)
- [16] Bar-Cohen, Y. (2001). *Electroactive polymer (EAP) actuators as artificial muscles: Reality, potential, and challenges* (2nd ed.). USA: SPIE Press.
- [17] Tomori, H., & Nakamura, T. (2011). Theoretical comparison of McKibben – Type artificial muscle and novel straight-fiber-type artificial muscle. *International Journal of Automation Technology*, 5(4), 544. <https://doi.org/10.20956/ijat.2011>
- [18] Gupta, U., Qin, L., Wang, Y., Godaba, H., & Zhu, J. (2019). Soft robots based on dielectric elastomer actuators: A review. *Smart Materials and Structures*, 28, 10. <https://doi.org/10.1088/1361-665X/ab3a77>
- [19] Saint-Aubin, C., Rosset, S., Schlatter, S., & Shea, H. (2018). High-cycle electromechanical aging of dielectric elastomer actuators with carbon-based electrodes. *Smart Materials and Structures*, 27(7). <https://doi.org/10.1088/1361-665X/aa9f45>

- [20] Niitake, J. (2020). Soft robotics using the dielectric elastomer actuator. *Measurement and Control*, 59(11), 841–846. <https://doi.org/10.11499/sicejl.59.841>
- [21] Koenigsdorff, M., Liebscher, H., Osipov, P., Mersch, J., & Gerlach, G. (2024). Influence of active-to-passive ratio on the deformation in circular dielectric elastomer actuators. *Micromachines*, 15(1), 125. <https://doi.org/10.3390/mi15010125>
- [22] Chiba, S., Waki, M., Jiang, C., Takeshita, M., Uejima, M., Arakawa, K., & Ohshima, K. (2021). The possibility of a high-efficiency wave power generation system using dielectric elastomers. *Energies*, 14, 3414. <https://doi.org/10.3390/en14123414>
- [23] Bose, H., & Fub, E. (2014). Novel dielectric elastomer sensors for compression load detection. In *Proceedings of the SPIE; Smart Structure and Material + Nondestructive Evaluation and Health Monitoring*, 905614. <https://doi.org/10.1117/12.204513>
- [24] Bose, H., & Ehrlich, J. (2023). Dielectric elastomer sensors with advanced designs and their applications. *Actuators*, 12, 115. <https://doi.org/10.3390/act12030115>
- [25] Zhu, Y., Giffney, T., & Aw, K. (2022). A dielectric elastomer-based multimodal capacitive sensor. *Sensors*, 22(2), 622. <https://doi.org/10.3390/s22020622>
- [26] Singh, N., Nakashima, K., & Shibata, T. (2020). Dielectric elastomer based stretchable textile sensor for capturing motion. In *Proceedings of the SPIE 11375, Electroactive Polymer Actuators and Devices (EAPAD) XXII*, 113752L. <https://doi.org/10.1117/12.2565743>
- [27] Chiba, S., & Waki, M. (2023). Excellent miniature thin film dielectric elastomer sensors for robot fingers used in human-robot interaction. *Archives of Advanced Engineering Science*, 1–13. <https://doi.org/10.47852/bonviewAAES32021716>
- [28] Kessel, V., Watzel, R., & Bauer, P. (2015). Analyses and comparison of an energy harvesting system for dielectric elastomer generators using a passive harvesting concept: The voltage-clamped multi-phase system. In *Proceedings of the SPIE; 9430, Smart Structures and Materials+ Nondestructive Evaluation and Health Monitoring, International Society for Optics and Photonics*, 943006. <https://doi.org/10.1117/12.2084316>
- [29] Zhao, Y., Yin, L., Zhong, S., Zha, J., & Dang, Z. (2020). Review of dielectric elastomers for actuators, generators and sensors. *IET Nanodielectrics*, 3(4), 99–106. <https://doi.org/10.1049/iet-nde.2019.0045>
- [30] Hu, P., Huang, Q., Madsen, J., & Skov, A. (2020). Soft silicone elastomers with no chemical cross-linking and unprecedented softness and stability. In *Proceedings of the SPIE; 11375, Electroactive Polymer Actuators and Devices (EAPAD) XXII*, 1137517. <https://doi.org/10.1117/12.2557003>
- [31] Skov, L., Bejenariu, G., Bøgelund, J., Benslimane, M., & Daugaard, E. (2012). Influence of micro and nanofillers on electro-mechanical performance of silicone EAPs. In *Proceedings of the SPIE; International Society for Optical Engineering*, 8340, 83400M. <https://doi.org/10.1117/12.966008>
- [32] Sikulskyi, S., Zefu, R., Govindarajan, S., Mekonnen, D., Madiyar, F., & Kim, D. (2022). Additively manufactured unimorph dielectric elastomer actuators with ferroelectric particles for enhanced low-voltage actuation. In *Proceedings of the SPIE; 12042, Electroactive Polymer Actuators and Devices (EAPAD) XXIV*, 120420W. <https://doi.org/10.1117/12.2613128>
- [33] Liebscher, H., Tahir, M., Wiessner, S., & Gerlach, G. (2022). Effect of barium titanate particle filler on the performance of polyurethane-based dielectric elastomer actuators. In *Proceedings of the SPIE; 12042, Electroactive Polymer Actuators and Devices (EAPAD) XXIV*, 120421. <https://doi.org/10.1117/12.2612354>
- [34] Carmel, M. (2020). Enhancing the permittivity of dielectric elastomers with liquid metal. In *Proceedings of the SPIE; Electroactive Polymer Actuators and Devices (EAPAD) XXII*, 11375-15. <https://doi.org/10.1117/12.2558951>
- [35] Hubertus, J., Croce, S., Neu, J., Seelecke, S., & Rizzello, G. (2023). Laser structuring of thin metal films of compliant electrodes on dielectric elastomers. *Advanced Functional Material*, 35(16), 2214176. <https://doi.org/10.1002/adfm.20221416>
- [36] Fasolt, B., Albuquerque, F., Hubertus, J., Schultes, G., Shea, H., & Seelecke, S. (2023). Electrode impact on the electrical breakdown of dielectric elastomer thin films. *Polymer*, 15, 4071. <https://doi.org/10.3390/polym15204071>
- [37] Willian, T., Bruch, D., Rizzello, G., Motzki, P., & Seelecke, S. (2024). Effects of solvents on the material properties of screen-printed electrodes and a PDMS dielectric for dielectric elastomer transducers. *Advanced Engineering Materials*, 26(10), 2301736. <https://doi.org/10.1002/adem.202301736>
- [38] McKay, T., O'Brien, B., Calius, E., & Anderson, I. (2011). Soft generators using dielectric elastomers. *Applied Physics Letters*, 98(14), 142903.
- [39] Anderson, I., Gisby, T., McKay, T., O'Brien, B., & Calius, E. (2012). Multi-functional dielectric elastomer artificial muscles for and smart machines. *Journal of Applied Physics*, 112(4), 041101.
- [40] Sanai, Y., & Shimamoto, H. (2022). Relationship between Cock Croft Walton Circuit, which aims for AED miniaturization, and discharge. In *Proceedings of 75th Electrical and Information-related Society; Kyushu Branch Federation*, 02-2P-02.
- [41] Wingert, A., Lichter, M., & Dubowsky, S. (2006). On the design of large degree-of-freedom digital mechatronic devices based on bistable dielectric elastomer actuators. *IEEE/ASME Transactions on Mechatronics*, 11(4), 448–456. <https://doi.org/10.1109/TMECH.2006.878542>
- [42] Conn, A., & Rossiter, J. (2012). Towards holonomic electro-elastomer actuators with six degrees of freedom. *Smart Materials and Structures*, 21(3), 035012. <https://doi.org/10.1088/0964-1726/21/3/035012>
- [43] McGough, K., Ahmed, S., Frecker, M., & Ounaies, Z. (2014). Finite element analysis and validation of dielectric elastomer actuators used for active origami. *Smart Material and Structure*, 23(9), 094002. <https://doi.org/10.1088/0964-1726/23/9/094002>
- [44] Chen, Y., Zhao, H., Mao, J., Chirarattananon, P., Helbling, E., Hyun, N., . . . , & Wood, R. (2019). Controlled flight of a microrobot powered by soft artificial muscles. *Nature*, 575(7782), 324–329. <https://doi.org/10.1038/s41586-019-1737-7>
- [45] Kumamoto, H., Hayashi, T., Yonemura, Y., Okuni, M., & Nalamura, T. (2020). Development of a locomotion robot using deformable dielectric elastomer actuator without pre-stretch. In *Proceedings of the SPIE 11375, Electroactive Polymer Actuators and Devices (EAPAD) XXII*, 1137509. <https://doi.org/10.1117/12.2558422>
- [46] Carpi, F., Frediani, G., Gerboni, C., Gemignani, J., & Rossi, D. (2014). Enabling variable-stiffness hand rehabilitation orthoses with dielectric elastomer transducers. *Medical Engineering & Physics*, 36(2), 205–211. <https://doi.org/10.1016/j.medengphy.2013.10.015>
- [47] Calabrese, L., Frediani, G., Gei, M., Rossi, D., & Carpi, F. (2018). Active compression bandage made of electroactive elastomers. *IEEE/ASME Transactions on Mechatronics*, 99, 1–1. <https://doi.org/10.1109/TMECH.2018.2860789>

- [48] Brochu, P., Yuan, W., Zhang, H., & Pei, Q. (2009). Dielectric elastomers for direct wind-to-electricity power generation. In *Proceedings of the ASME; 2009 Conference on Smart Materials, Adaptive Structures and Intelligent System*, 197–204. <https://doi.org/10.1115/SMASIS2009-1335>
- [49] Di, K., Bao, K., Chen, H., Xie, X., Tan, J., Shao, Y., . . . , & Shiju, E. (2021). Dielectric elastomer generator for electromechanical energy conversion: A mini review. *Sustainability*, 13, 9881. <https://doi.org/10.3390/su13179881>
- [50] Jean-Mistral, C., Basrou, S., & Chaillout, J. (2008). Dielectric polymer: Scavenging energy from human motion. In *The Proceedings of SPIE, Electroactive Polymer Actuators and Devices (EAPAD)*, 6927, 692716. <https://doi.org/10.1117/12.776879>
- [51] Cao, J., Guo, Z., Shiju, E., Zhao, T., & Gao, Z. (2022). Generation performance of self-biased dielectric elastomer generator based on charge pump circuit. *AIP Advances*, 12, 095001. <https://doi.org/10.1063/5.0092175>
- [52] Guan, T., Wang, W., Wang, X., Wen, C., Xu, R., Zhu, C., . . . , & Wang, H. (2023). Corrugation-like triboelectric nanogenerators integrated buoys for wave energy harvesting. *Journal of Physics: Conference Series*, 2592, 012052. <https://doi.org/10.1088/1742-6596/2592/1/012052>
- [53] Du, X., Du, L., Li, P., Liu, X., Han, Y., Yu, H., . . . , & Tang, L. (2023). A dielectric elastomer and electret hybrid ocean wave power generator with oscillating water column. *Nano Energy*, 111, 108417. <https://doi.org/10.1016/j.nanoen.2023.108417>
- [54] Chiba, S., Waki, M., Wada, T., Hirakawa, Y., Masuda, K., & Ikoma, T. (2013). Consistent ocean wave energy harvesting using electroactive polymer (dielectric elastomer) artificial muscle generators. *Applied Energy*, 104, 497–502. ISSN 0306-2619. <https://doi.org/10.1016/j.apenergy.2012.10.052>
- [55] Miyazaki, T., & Osawa, H. (2007). Search report of wave power devices. In *The 2007 Spring Conference of the Japan Society of Naval Architects and Ocean Engineers*, 4, 43–46.
- [56] Srinu, D., Venkateswarlu, V., Vijay, G., & Atmanand, A. (2024). Hydrodynamic analysis of oscillating water column in the presence of seabed undulations. *Journal of Marine Science and Technology*, 29, 404–417. <https://doi.org/10.1007/s00773-024-00994-5>
- [57] Mohapatra, P., Vijay, G., Bhattacharyya, A., & Sahoo, T. (2023). Influence of distinct bottom geometries on the hydrodynamic performance of an OWC device. *Energy*, 277, 127605. <https://doi.org/10.1016/j.energy.2023.127605>
- [58] Energy Domain Special Feature. (2023). Achievement the world's highest thermal efficiency and high flexibility Joetsu thermal power station unit no.1, Tohoku Electric Power Co. *Mitsubishi Heavy Industries Technical Review*, 60(3), 1–6. <https://www.mhi.co.jp/technology/review/pdf/603/603130.pdf>
- [59] Anderlini, E., Thomas, G., Husain, S., & Parker, G. (2020). Towards real-time reinforcement learning control of a wave energy converter. In *Proceedings of the ASME 2020 39th International Conference on Ocean, Offshore and Arctic Engineering OMAE2020*, 8(11), 845.
- [60] Hiratsuka Power Plant. (2020). *Hiratsuka Energy Research Association*. Retrieved from: <https://www.city.hiratsuka.kanagawa.jp/common/200074600.pdf>

**How to Cite:** Chiba, S., & Waki, M. (2024). A Marine Experiment Using Dielectric Elastomer Generators and Comparative Study with Actual Measured Values and Theoretical Values. *Archives of Advanced Engineering Science*. <https://doi.org/10.47852/bonviewAAES42023530>